# Substrate Recognition and Saturation Kinetics in de Novo Designed Histidine-Based Four-Helix Bundle Catalysts

**Kerstin S. Broo, Helena Nilsson, Jonas Nilsson, and Lars Baltzer***

*Contribution from the Department of Chemistry, Göteborg University, 41296 Göteborg, Sweden*

*Received March 2, 1998*

**Abstract:** Designed four-helix bundle proteins with reactive sites based on the cooperativity of $HisH^+$−His pairs in helical sequences catalyze acyl-transfer reactions of *p*-nitrophenyl esters with large rate enhancements. The function of the $HisH^+$−His site has been expanded by the introduction of flanking residues to provide recognition of substrate carboxylate and hydrophobic residues. The second-order rate constants for the MN-42 catalyzed hydrolysis of *p*-nitrophenyl acetate and of mono-*p*-nitrophenyl fumarate, under conditions of excess catalyst over substrate, in aqueous solution at pH 5.1 and 290 K are 0.030 $M^{-1}$ $s^{-1}$ and 0.027 $M^{-1}$ $s^{-1}$, respectively. The reactive site of MN-42 contains only histidine residues. The sequence of MNKR is the same as that of MN-42 except that one Lys and one Arg residue have been introduced in the adjacent helix to flank the $HisH^+$−His site and the resulting second-order rate constants are 0.075 $M^{-1}$ $s^{-1}$ and 0.135 $M^{-1}$ $s^{-1}$. MNKR catalyzed hydrolysis of the fumarate follows saturation kinetics with a $k_{cat}/K_M$ of 0.17 $M^{-1}$ $s^{-1}$ which is 230 times larger than the second-order rate constant of the 4-methyl imidazole catalyzed reaction. The second-order rate constants for the JNIII catalyzed hydrolysis of *p*-nitrophenyl acetate and of *p*-nitrophenyl valerate are 0.007 $M^{-1}$ $s^{-1}$ and 0.097 $M^{-1}$ $s^{-1}$, respectively, and binding of the aliphatic group increases the rate constant by more than one order of magnitude. Chiral recognition by de novo designed polypeptides has been demonstrated for the first time, and the hydrolysis of the *p*-nitrophenyl ester of D-norleucine has been catalyzed with a second-order rate constant that is twice as large as that of the L-norleucine ester.

## Introduction

The increasing number of reported de novo designed polypeptides with well-defined tertiary structures[1−6] suggest that the engineering of folded polypeptides, tailored for specific functions, is timely. The successful introduction of metal[7] and cofactor[8,9] binding sites and porphyrin binding pockets[10−12] and the development of peptides capable of forming ion channels[13] and nanotubes[14] are but a few examples of the diversity of applications that are being approached by the design of nonnatural amino acid sequences. Much attention is focused on the design of novel catalysts because of the remarkable efficiency and selectivity exhibited by the natural enzymes and because of the challenge involved in fine-tuning polypeptide structures with complex reactive sites for the purpose of obtaining cooperative catalysis.

Designed polypeptide catalysts with widely different catalytic mechanisms have now been reported where the relationship between structure and function is at least partly understood and that show rate enhancements of approximately 3 orders of magnitude. The decarboxylation of oxaloacetate has been accomplished by two 14-residue amphiphilic helical polypeptides, oxaldie1 and oxaldie2,[15] that aggregate in solution to form bundle-like structures. The reaction mechanism proceeds via covalent enamine formation, and the most efficient catalyst is oxaldie 1 mainly due to the low $pK_a$ of the amino terminal of the peptide. The peptides bind the dianionic substrate oxaloacetate with $K_M$ values in the millimolar range.

A synthetic peptide ligase has been designed which catalyses ligation reactions with rate enhancements of $4 \times 10^3$ over that of the background reaction.[16] The catalyst is a 33-residue amphiphilic helix that binds the reacting peptide fragments to increase the effective concentrations of electrophile and nucleophile with dissociation constants in the micromolar range. The reaction mechanism includes the attack of the side chain of the amino terminal Cys of the nucleophile peptide fragment on the activated thioester of the carboxy terminal of the electrophile peptide fragment, and the resulting thioester rearranges to yield the final amide product.[17]

* E-mail Lars.Baltzer@oc.chalmers.se.

(1) Hill, R. B.; DeGrado, W. F. *J. Am. Chem. Soc.* **1998**, *117*, 1138−1145.
(2) Dolphin, G. T.; Brive, L.; Johansson, G.; Baltzer, L. *J. Am. Chem. Soc.* **1996**, *118*, 11297−11298.
(3) Brive, L.; Dolphin, G. T.; Baltzer, L. *J. Am. Chem. Soc.* **1997**, *119*, 8598−9607.
(4) Struthers, M. D.; Cheng, R. P.; Imperiali, B. *Science* **1996**, *271*, 342−345.
(5) Betz, S. F.; DeGrado, W. F. *Biochemistry* **1996**, *35*, 6955−6962.
(6) Bassil, D. I.; Mayo, S. L. *Science* **1997**, *278*, 82−87.
(7) Walkup, G. K.; Imperiali, B. *J. Am. Chem. Soc.* **1996**, *118*,3053−3054.
(8) Roy, R. S.; Imperiali, B. *Tetrahedron Lett.* **1996**, *37*,2129−2132.
(9) Mihara, H.; Tomizaki, K.; Nishino, N.; Fujimoto, T. *Chem. Lett.* **1993**, 1533−1536.
(10) Rabanal, F.; DeGrado, W. F.; Dutton, P. L. *J. Am. Chem. Soc.* **1996**, *118*, 473−474.
(11) Nastri, F.; Lombardi, A.; Morelli, G.; Maglio, O.; D'Auria, G.; Pedone, C.; Pavone, V. *Chem. Eur. J.* **1997**, *3*, 340−349.
(12) Mihara, H.; Tomizaki, K.; Fujimoto, T.; Sakamoto, S.; Aoyagi, H.; Nishino, N. *Chem. Lett.* **1996**, *3*, 187−188.
(13) Lear, J. D.; Schneider, J. P.; Kienker, P. K.; DeGrado, W. F. *J. Am. Chem. Soc.* **1997**, *119*, 3212−3217.
(14) Hartgerink, J. D.; Granja, J. R.; Milligan, R. A.; Ghadiri, M. R. *J. Am. Chem. Soc.* **1996**, *118*, 43−50.
(15) Johnsson, K.; Allemann, R. K.; Widmer, H.; Benner, S. A. *Nature* **1993**, *365*, 530−532.
(16) Severin, K.; Lee, H. D.; Kennan, A. J.; Ghadiri, M. R. *Nature* **1997**, *389*, 706−709.
(17) Dawson, P. E.; Muir, T. W.; Clark-Lewis, I.; Kent, S. B. H. *Science* **1994**, *266*, 776−779.

S0002-7863(98)00682-9 CCC: $15.00 
Published on Web 09/25/1998

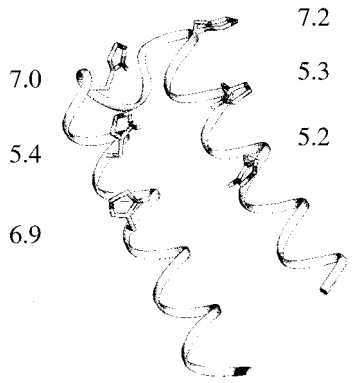


**Figure 1.** Modeled structure of KO-42. The histidine side chains are shown with their corresponding p$K_a$ values. KO-42 is a symmetric dimer, but only the monomer is shown for reasons of clarity of presentation. The *i, i+4, i+8* configuration ensures that the geometric relationship between each His pair is similar.

KO-42, a designed antiparallel helix-loop-helix hairpin dimer with 42 residues in the monomer sequence, catalyses acyl-transfer reactions of *p*-nitrophenyl esters. The reactive site contains six His residues (Figure 1),[18] and the reaction mechanism proceeds via rate-limiting formation of an acyl-imidazoyl intermediate followed by attack on the acyl intermediate by the appropriate nucleophile to form the reaction products. The second-order rate constant for the hydrolysis of mono-*p*-nitrophenyl fumarate at pH 4.1 is 1140 times larger than that of the 4-methylimidazole catalyzed reaction. The rate enhancement at low pH originates from cooperative nucleophilic and general acid catalysis by unprotonated nucleophilic histidines (*i*) flanked by protonated histidines (*i-4*) in a helical segment.[19]

The reported catalysts demonstrate that it has been possible to accomplish by rational design large catalytic rate enhancements for chemical reactions of great diversity. The engineering of reactive sites capable of substrate discrimination is thus the next step in catalyst design. We now wish to report that the recognition of carboxylate and hydrophobic residues of *p*-nitrophenyl esters has been accomplished in catalysts derived from KO-42, where the $HisH^+-His$ site has been expanded by the introduction of flanking Arg and Lys residues. The results demonstrate the feasibility of engineering selective reactive sites in the further development of designed polypeptide catalysts.

## Results

**Design and Tertiary Structures of Four-Helix Bundle Catalysts.** The amino acid sequences of KO-42 and the polypeptides reported here were based on that of the previously reported de novo designed template polypeptide SA-42 that folds into a helix-loop-helix motif and dimerizes to form a four-helix bundle.[20] In short, the choice of amino acid residues was based on their propensities for secondary structure formation,[21,22] and residues were also introduced that could stabilize the folded structure by capping, stabilization of the helical dipoles, and intrahelical salt bridge formation.[23] The driving forces for hairpin formation are the hydrophobic interactions between amphiphilic helices, and the hydrophobic core was therefore designed in a shape-complementary way from leucines, norleucines, phenylalanines, a valine, and an isoleucine residue.

1 19
Ac-N-A-A-D-Nle-E-A-A-I-K-**H**-L-A-E-**H**-Nle-A-A-**H**-

20 23
-G-P-V-D-

42 24
$NH_2$-G-A-R-A-F-A-E-F-**H**-K-A-L-**H**-E-A-Nle-**H**-A-A-

**KO-42**

| peptide | 8 | 11 | 15 | 19 | 26 | 30 | 34 | $k_2$ (**I**) $M^{-1}$ $s^{-1}$ | $k_2$ (**II**) $M^{-1}$ $s^{-1}$ |
|---|---|---|---|---|---|---|---|---|---|
| KO-42 | A | **H** | **H** | **H** | **H** | **H** | **H** | 0.310 | 0.290 |
| SA-42 | A | A | **H** | K | Q | Q | A | - | - |
| MN-42 | A | **H** | **H** | **H** | Q | Q | A | 0.027 | 0.030 |
| JN-42 | A | A | Q | K | **H** | **H** | **H** | 0.065 | - |
| MNI | A | **H** | **H** | Q | Q | Q | A | 0.011 | - |
| MNII | A | A | **H** | **H** | Q | Q | A | 0.008 | - |
| MNKK | A | **H** | **H** | **H** | Q | K | K | 0.068 | 0.086 |
| MNRR | A | **H** | **H** | **H** | Q | R | R | 0.080 | 0.049 |
| MNKR | A | **H** | **H** | **H** | Q | K | R | 0.135 | 0.075 |
| MNRK | A | **H** | **H** | **H** | Q | R | K | 0.110 | 0.106 |
| MNKQ | A | **H** | **H** | **H** | Q | K | Q | 0.034 | 0.031 |
| MNQK | A | **H** | **H** | **H** | Q | Q | K | - | - |
| MNRQ | A | **H** | **H** | **H** | Q | R | Q | 0.058 | 0.073 |
| MNQR | A | **H** | **H** | **H** | Q | Q | R | 0.066 | 0.056 |
| MNEE | A | **H** | **H** | **H** | Q | E | E | 0.018 | 0.022 |
| MNOrnR | A | **H** | **H** | **H** | Q | Orn | R | 0.092 | 0.081 |
| JNI | A | A | Q | K | **H** | **H** | A | 0.010 | - |
| JNII | A | A | Q | K | Q | **H** | **H** | 0.055 | 0.048 |
| JNIII | A | A | Q | K | **H** | Q | **H** | 0.007 | - |
| JNIIRR | A | R | R | K | Q | **H** | **H** | 0.105 | 0.067 |
| $JNIIK_8R_{11}$ | K | R | Q | K | E | **H** | **H** | 0.065 | 0.039 |
| $JNIIR_8K_{11}$ | R | K | Q | K | E | **H** | **H** | 0.055 | 0.018 |

**Figure 2.** Amino acid sequences of KO-42 and related peptides listed in the one-letter code and Nle for norleucine. The sequences of related peptides are the same as that of KO-42 except for positions 8, 11, 15, 19, 26, 30, and 34 where the amino acid residues presented have replaced those of the original sequence. His residues are shown in bold. The second-order rate constants are those for the hydrolysis of **I** and **II** in aqueous solution at pH 5.1 and 290 K catalyzed by the listed peptide catalysts. The corresponding rate constants for the 4-MeIm catalyzed reactions are 0.000 74 $M^{-1}$ $s^{-1}$ (**I**) and 0.000 72 $M^{-1}$ $s^{-1}$ (**II**).

The primary amino acid sequence was varied extensively to simplify the assignment of the $^1H$ NMR spectrum, and two NOE reporter groups, the phenyl rings of Phe-35 and Phe-38, were incorporated at the lower part of helix II to facilitate identification of hairpin formation and to induce chemical shift dispersion.[20] The full charges of the amino and the carboxy terminals of SA-42 were neutralized in KO-42 by acetylation and amidation. In the design of the His based acyl-transfer catalyst KO-42, Ala-11, Lys-19, Gln-26, Gln-30 and Ala-34 of SA-42 were replaced by five histidines (Figure 2).[18]

SA-42 and KO-42 have been characterized extensively by $^1H$ NMR and CD spectroscopy and equilibrium sedimentation ultracentrifugation.[18,24] The CD spectra of SA-42 and KO-42 both show the negative maxima at 208 and 222 nm that are characteristic of helical peptides. The mean residue ellipticities at 222 nm is $-24\,000 \pm 1000$ deg $cm^2$ $dmol^{-1}$ for KO-42 and $-25\,000 \pm 1000$ deg $cm^2$ $dmol^{-1}$ for SA-42, corresponding to helical contents of 60−70%.[25,26] The magnitudes of these mean residue ellipticities are among the highest of those reported for

(18) Broo, K. S.; Brive, L.; Ahlberg, P.; Baltzer, L. *J. Am. Chem. Soc.* **1997**, *119*, 11362−11372.
(19) Broo, K. S.; Nilsson, H.; Nilsson, J.; Flodberg, A.; Baltzer, L.; *J. Am. Chem. Soc.* **1998**, *120*, 4063−4068.
(20) Olofsson, S.; Johansson, G.; Baltzer, L. *J. Chem. Soc., Perkin Trans. 2* **1995**, 2047−2056.
(21) Chou, P. Y.; Fasman, G. D. *Biochemistry* **1974**, *13*, 211−222.
(22) Chou, P. Y.; Fasman, G. D. *Biochemistry* **1974**, *13*, 222−244.
(23) Bryson, J. W.; Betz, S. F.; Lu, H. S.; Suich, D. J.; Zhou, H. X.; O'Neil, K. T.; DeGrado, W. F. *Science* **1995**, *270*, 935−941.
(24) Olofsson, S.; Baltzer, L. *Folding Des.* **1996**, *1*, 347−356.
(25) Broo, K. S.; Sott, R.; Brive, L.; Baltzer, L. *Folding Des.* **1998**, *3*, 303−312.
(26) Chen, Y.-H.; Yang, J. T.; Chau, K. H. *Biochemistry*, **1974**, *13*, 3350−3359.

**Scheme 1**

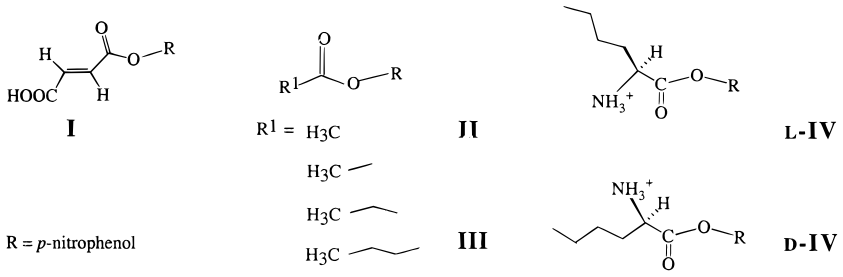


helical polypeptides of this size. The $^1$H NMR spectra of both peptides have been assigned, and their secondary structures have been identified by medium range NOEs and αH chemical shift deviations from random coil values. Although an atomic resolution structure is not yet available, equilibrium sedimentation ultracentrifugation and diagnostic long-range NOEs show that both KO-42 and SA-42-fold into antiparallel hairpin dimers.

The amino acid sequences of the peptides reported here differ from those of the sequences of SA-42 or KO-42 by two to four residues (Figure 2). The CD spectra of the polypeptides show negative maxima at 208 and 222 nm, and the measured mean residue ellipticities at 222 nm range from −18 000 to −25 000 deg cm$^2$ dmol$^{-1}$. On the basis of the similarity of the primary sequences and the measured mean residue ellipticities, the polypeptides presented here are assumed to fold into antiparallel hairpin helix-loop-helix dimers, although full structural analysis of each one has not been carried out.

**Reactive Sites Based on the HisH$^+$−His Amino Acid Pair.** In the pursuit of the basic building block for the construction of His-based catalysts, the cooperative two-residue HisH$^+$−His site was identified.[19] As a result of the identification and incorporation of the reactive entities of KO-42 in separate peptides, the second-order rate constants of each one could be measured (Figure 2). It was deduced that the reactivities of the HisH$^+$−His sites are mainly controlled by the p$K_a$'s of the participating histidines.[19] The p$K_a$ values of the peptides described here have been determined, and they can be affected by only a few tenths of a p$K_a$ unit by residues in the neighboring helix which induces only minor differences in reactivity.[27] However, substrate binding was also suggested from the kinetic measurements. The measured second-order rate constants for the reactions catalyzed by JN-42 and by MN-42, that contain the His residues of helix I and helix II of KO-42, respectively, do not add up to the second-order rate constant of KO-42. The second-order rate constant for the JN-42 catalyzed hydrolysis of mono-*p*-nitrophenyl fumarate (**I**) is 0.065 M$^{-1}$ s$^{-1}$ in aqueous solution at pH 5.1 and 290 K, and that of MN-42 is 0.027 M$^{-1}$ s$^{-1}$,[19] whereas that of KO-42 is 0.31 M$^{-1}$ s$^{-1}$ under the same conditions. The lack of additivity suggested that protonated histidines could contribute in a cooperative fashion to transition-state binding in reactions catalyzed by His residues in the adjacent helix.

A small peptide library, based on the peptide MN-42, was therefore designed, where positively charged arginines and lysines were introduced in positions 30 and 34 in helix II for the purpose of stabilizing the developing oxyanion in the transition state preceding the acyl intermediate. The peptides with all possible combinations of Arg, Lys, and Gln residues in positions 30 and 34 in helix II were synthesized, and one peptide was also designed on the basis of the reactivity of the most efficient two-residue site in helix II, that of JNII. In JNIIRR that contains His-30 and His-34, two Arg were introduced in positions 11 and 15. MN-42 and JNII were used as reference peptides, and a negative reference, MNEE with two Glu in positions 30 and 34 was also synthesized.

**The Reactivity of HisH$^+$−His Sites Flanked by Arg and Lys.** The second-order rate constants for the peptide catalyzed hydrolysis of **I** were determined under conditions of excess catalyst over substrate in aqueous solution at pH 5.1 and 290 K. Typical peptide concentrations were 0.25−0.4 mM with a concentration of **I** of 0.13 mM. Excellent first-order kinetics were observed, and as long as the concentration of substrate is smaller than the dissociation constant for the catalyst−substrate complex, i.e., [S] ≪ $K_S$, pseudo-first-order kinetics will be observed also for catalysts that show saturation kinetics. The second-order rate constants were determined by measuring the slope of the plot of the pseudo-first-order rate constant versus [**I**].

The introduction of flanking Arg and Lys residues in peptides that contain reactive His sites in the adjoining helix increased their catalytic efficiency (Figure 2). The second-order rate constants for the MNKR catalyzed hydrolysis of **I** is 0.135 M$^{-1}$ s$^{-1}$, a factor of 5 larger than that of the MN-42 catalyzed reaction, which is 0.027 M$^{-1}$ s$^{-1}$, and the JNIIRR catalyzed reaction is 0.105 M$^{-1}$ s$^{-1}$, which is almost twice as large as 0.055 M$^{-1}$ s$^{-1}$, the rate constant for the JNII catalyzed reaction.

**Recognition of a Negatively Charged Substrate and Binding of the Developing Oxyanion in the Transition State Preceding the Acyl Intermediate.** To probe the modes of interaction, *p*-nitrophenyl acetate (**II**), which does not contain the negatively charged carboxylate residue of **I,** was used as a substrate (Scheme 1) because, in the hydrolysis of **II**, any observed rate enhancement upon introduction of positively charged side chains are most likely due to interactions with the developing oxyanion in the transition state. The second-order rate constant for the hydrolysis of **II** increased upon the introduction of flanking Arg and Lys in comparison with those of the reactions catalyzed by peptides that only contained HisH$^+$−His sites. Consequently, the developing oxyanion was stabilized by the side chains of the flanking residues.

KO-42, MN-42, and JNII did not show any discrimination between **I** and **II**; the second-order rate constants were the same for both substrates. However, upon introduction of Arg or Lys in helix II, the peptides catalyzed the hydrolysis of **I** with larger rate constants than they catalyzed the hydrolysis of **II**, showing that the fumaryl residue is bound by the introduced residues. The observed second-order rate constants for MNKR catalyzed hydrolysis of **I** and **II** are 0.135 M$^{-1}$ s$^{-1}$ and 0.075 M$^{-1}$ s$^{-1}$, respectively. Interestingly, reversing the positions of the Arg and Lys residues in the sequence of MNKR gives rise to a peptide that is incapable of recognizing the fumaryl residue since the second-order rate constants for MNRK catalyzed hydrolysis of **I** and **II** are the same, 0.110 M$^{-1}$ s$^{-1}$ and 0.106 M$^{-1}$ s$^{-1}$.

(27) Engel, M.; Williams, R. W.; Erickson, B. W. *Biochemistry* **1991**, *30*, 3161−3169.

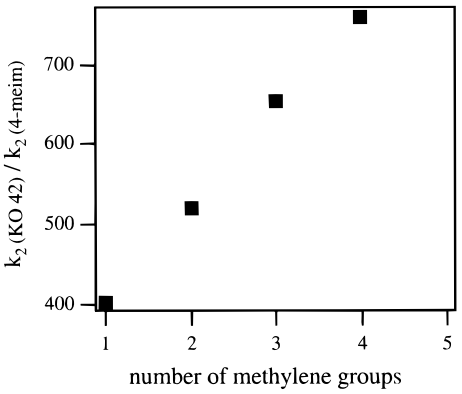


**Figure 3.** Ratio $k_2$ (KO-42)/$k_2$ (4-MeIm) at pH 5.1 and 290K as a function of the number of methylene and methyl groups of the fatty acid ester substrate.

Replacing Lys-30 by an ornithine (Orn) that has a shorter side chain by one methylene group gives rise to a peptide that does not discriminate between **I** and **II**. The rate constants are again the same within experimental accuracy, and the interactions between the catalyst and the fumaryl carboxylate anion substrate are therefore specific. The second-order rate constant for the MNOrnR catalyzed hydrolysis of **I** is 0.092 $M^{-1}$ $s^{-1}$ and that of the MNOrnR catalyzed hydrolysis of II is 0.081 $M^{-1}$ $s^{-1}$. The negative reference peptide MNEE does, in fact, show a small decrease in the second-order rate constants compared to that of MN-42, suggesting that, in this case, the fumaryl carboxylate anion is repelled. The rate constant of MNEE catalyzed hydrolysis of **I** is even smaller than that of **II**, in agreement with the suggestion of repulsion of the carboxylate anion by the negatively charged Glu's, although in this case, the differences are probably within experimental error.

To probe the geometry and specificity of the reactive site, the second-order rate constant of JNIIRR catalyzed hydrolysis of **I** was compared to that of $JNIIK_8R_{11}$ and $JNIIR_8K_{11}$ (Figure 2). All three peptides have the same reactive histidine entity, $HisH^+$-30 −His-34 and two flanking positively charged residues; however, in the sequence of JNIIRR the flanking residues are Arg-11 and Arg-15, whereas in the latter two sequences the flanking residues are Arg and Lys located in positions 8 and 11, i.e. they have been moved one turn of the helix toward the N terminus of helix I. The second-order rate constants for the hydrolysis of **I** show that there is binding of neither the developing oxyanion nor the fumaryl carboxylate in the peptides $JNIIK_8R_{11}$ and $JNIIR_8K_{11}$ as the rate constants are approximately the same as, or smaller than, that of JNII which has no flanking residues.

**Recognition of Hydrophobic Substrates.** The helix-loop-helix hairpin motif is formed mainly due to the hydrophobic interactions between amphiphilic helices. To probe whether the hydrophobic core would be partly exposed and available for hydrophobic binding of substrates, the rate constants for hydrolysis of a series of straight chain fatty acid *p*-nitrophenyl esters were measured (Scheme 1). The *p*-nitrophenyl acetate, propionate, butyrate, and valerate were studied, whereas *p*-nitrophenyl caproate was only sparsely soluble under the reaction conditions and did not provide good kinetic measurements due to precipitation.

The rate of KO-42 catalyzed ester hydrolysis, rather than the logarithmic rate, increased almost linearly with the number of methylene groups in the alkyl side chain (Figure 3), which means that the free energy gain in increasing the chain length tends toward a maximum value. The second-order rate constants

**Table 1.** Second-Order Rate Constants and Ratios of Second-Order Rate Constants for Peptide and 4-MeIm Catalyzed Hydrolysis of III at pH 5.1 and 290 K

| peptide | $k_2$ (**III**) $M^{-1}$ $s^{-1}$ | $k_2$ (III)/$k_2$ (I) | $k_2$ (III)/$k_2$ (II) |
|---|---|---|---|
| KO-42 | 0.535 | 1.7 | 1.8 |
| JNI | 0.027 | 2.8 | |
| JNII | 0.186 | 3.4 | 3.9 |
| JNIII | 0.097 | 14.0 | |
| JNIIRR | 0.144 | 1.4 | 2.1 |
| 4-MeIm | 0.00070 | 0.95 | 0.95 |

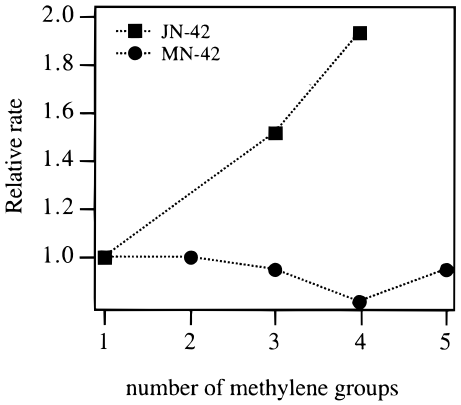


**Figure 4.** Rates of hydrolysis of fatty acid esters at pH 5.1 and 290 K, catalyzed by MN-42 (circle) and JN-42 (square), relative to those of *p*-nitrophenyl acetate. The relative rates have been determined by using the same stock peptide solution for each substrate.

increased from 0.29 $M^{-1}$ $s^{-1}$ to 0.54 $M^{-1}$ $s^{-1}$ as a function of chain length in the series from *p*-nitrophenyl acetate (**II**) to *p*-nitrophenyl valerate (**III**) at pH 5.1 and 290 K (Table 1). Binding of the hydrophobic alkyl chain of the esters differs between the catalysts MN-42 and JN-42. The reactive site of JN-42 showed substantial rate enhancements, whereas the rate constants for the MN-42 catalyzed reactions were not affected by the structure of the substrate (Figure 4), suggesting the presence of specific alkyl chain binding sites.

To identify the hydrophobic binding site for the JN-42 catalyzed reactions, the second-order rate constants for the hydrolysis of *p*-nitrophenyl valerate (**III**) catalyzed by JNI, JNII, and JNIII were measured (Table 1) and compared to those for the hydrolysis of **I** that does not have a hydrophobic residue. The second-order rate constants for JNII catalyzed hydrolysis of **I** and **II** do not differ by more than 10%, but the second-order rate constants for JNIII catalyzed hydrolysis of **III** and **I** are 0.097 $M^{-1}$ $s^{-1}$ and 0.007 $M^{-1}$ $s^{-1}$, respectively. At pH 5.1, the catalytic activity of JNIII is due solely to nucleophilic attack by His-34,[18] and the rate enhancement is therefore due to the binding of the hydrophobic alkyl residue by the peptide. The rate enhancements by JNI and JNII are smaller, JNI showed a ratio $k_2$ (**III**)/$k_2$ (**I**) of 2.8, and JNII showed a ratio of $k_2$ (**III**)/$k_2$ (**I**) of 3.4. The existence of a hydrophobic binding pocket in close proximity to His-34 is compatible with the fact that the side chain of His-34 appears to be partly buried in the hydrophobic core of the folded four-helix bundle. The proximity of His-34 to the hydrophobic core was confirmed by NOE connectivities between the $\beta$ protons of His-34 and the methyl groups of Leu-12, Leu-31, and Nle's that were identified in the $^1$H NMR NOESY spectrum of JNIII (Figure 5). The reason that the hydrophobic binding pocket is not exploited to its full potential in the JNII catalyzed reaction may be that the constraints imposed on the structure of the transition state by the geometry of the His reactive site prevent the alkyl side chain from binding in an optimal way.

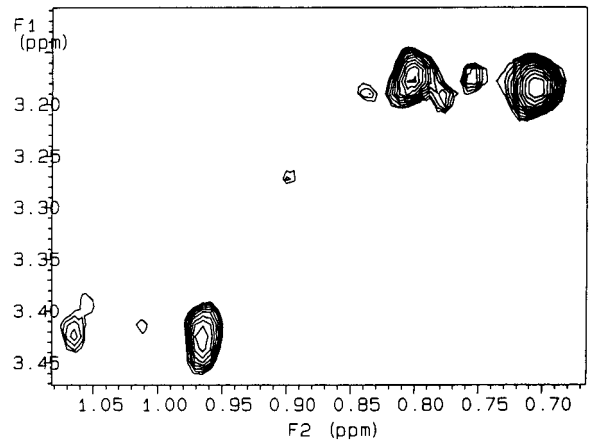


**Figure 5.** Part of the $^1$H NMR NOESY spectrum of JNIII in 10 vol % TFE-$d_3$ in $H_2O/D_2O$ (90:10) showing NOE connectivities between $\beta$-protons of His-34 at 3.18 ppm and the methyl groups of Leu-12 at 0.84 ppm and those of Leu-31 at 0.71 ppm. The cross-peak at 0.78 ppm is due to NOE connectivities between the $\beta$-protons of His-34 and the methyl groups of Ile-9 and or one or more of the norleucines, all of which overlap. The $\beta$-protons of His-26 at 3.42 ppm shows only cross-peaks to methyl groups of Val-22 at 0.96 and 1.06 ppm.

The possibility of making use of cooperative oxyanion and hydrophobic binding was investigated in the case of the JNIIRR catalyzed hydrolysis of **III** and compared to that of JNII that has no flanking arginines. The second-order rate constant at pH 5.1 and 290 K was 0.14 $M^{-1}$ $s^{-1}$, whereas that of the JNII catalyzed reaction was 0.19 $M^{-1}$ $s^{-1}$ (Table 1), showing that cooperative hydrophobic and charge−charge binding could not be achieved for JNIIRR.

**Chiral Recognition.** The introduction of positively charged amino acid residues in the helix adjacent to the one that carries the $HisH^+$−His site gives rise to recognition of a negatively charged substrate, and the peptides also have a demonstrated capacity for binding aliphatic residues. In combination with the stereochemistry of the $HisH^+$−His site, where the His with the highest number in the sequence is the nucleophile and the one with the lowest number is the general acid catalyst,[19] chiral recognition will be possible if these interactions can be exploited simultaneously in binding a substrate. The *p*-nitrophenyl esters of the enantiomers of Nle (L-**IV**, D-**IV**, Scheme 1) were used to probe chiral discrimination since they contain one alkyl and one charged substituent. An amino acid ester substrate with a negatively charged side chain, such as the Glu ester, would be preferable but is unsuitable due to the efficient intramolecularly catalyzed reaction. The positively charged amino acids in the adjacent helix could, however, potentially repel one enantiomer of the Nle substrates more readily than the other.

The second-order rate constants for the 4-MeIm catalyzed hydrolysis of the D- and L-Nle esters were found to be equal as were those of the background reactions in aqueous solution at pH 5.1 and 290K (Table 2). But, the rate constants for the reactions catalyzed by peptides with flanking positively charged amino acid residues were larger for the D-amino acid ester than for the L-amino acid ester. Peptide catalysts that contained no flanking residues did not discriminate between enatiomeric esters, and the difference between enantiomeric substrates was less for the catalysts with only one flanking charged residue than for the catalysts with two.

More pronounced chiral interactions would be expected from catalysis of reactions where the substrate side chains are bound rather than repelled. The catalysis of hydrolysis of the *p*-nitrophenyl esters of L- and D-Lys by MNEE was therefore attempted. However, the low reactivity of MNEE and the high inherent reactivity of the esters limited the possibilities for observing chiral discrimination.

**Table 2.** Rate Constant Ratios of Peptide Catalyzed Hydrolysis of L-**IV** and D-**IV** at pH 5.1 and 290 K

| peptide | $k_2$ (D-**IV**)/$k_2$ (L-**IV**) |
|---|---|
| KO-42 | 1.4 |
| MN-42 | 1.1 |
| JN-42 | 1.3 |
| MNKK | 2.0 |
| MNRR | 1.7 |
| MNKR | 1.7 |
| MNRK | 2.0 |
| MNKQ | 1.7 |
| MNRQ | 1.7 |
| MNQR | 1.4 |
| JNI | 1.4 |
| JNII | 1.3 |
| JNIII | 0.8 |

**Substrate Binding and Saturation Kinetics.** Natural enzymes bind their substrates and form enzyme−substrate complexes prior to the actual chemical transformations. In KO-42 catalyzed hydrolysis of **I**, no signs of substrate recognition or saturation kinetics were observed.[18] The number of possible reaction pathways in KO-42 catalysis is, however, large, and by designing more well-defined reactive sites, substrate recognition was achieved for MNKR, MNRR, and JNIIRR, implying that a smaller number of pathways were available in these reactions. The stronger binding of **I** in the transition state was also expected to lead to stronger binding in the ground state and perhaps give rise to a peptide−substrate complex along the reaction pathway which could be observed by the onset of saturation kinetics.

To detect a possible catalyst−substrate complex, a reaction is usually studied under conditions of excess substrate over catalyst, and the initial rates are plotted as a function of substrate concentration. The commonly used form of the Michaelis−Menten equation is derived under the assumption that $[S]_o$ is $\gg [E]_o$ so that [ES] can be neglected in comparison with [S] and $[S]_o$ be used as a measure of [S]. This is usually valid for natural enzymes where the catalytic efficiencies are high and the rates can be measured for small concentrations of catalyst. However, in the case of the catalysts described here, peptide concentrations on the order of 0.3−0.6 mM have to be used, while the substrate concentration due to solubility problems cannot be larger than approximately 2 mM and therefore in the range from 0.05 to 2 mM. The concentration of catalyst is clearly not negligible in comparison with that of the substrate. It is, however, possible to use the Michaelis−Menten equation without the simplifying assumption that $[S] \gg [E]$ which leads to an expression that has a square root dependence on the concentration of substrate, eq 1.

$$v = k_{cat}[PS] = k_{cat}(([P_0] + [S_0] + K_M)/2 - \sqrt{([P_0] + [S_0] + K_M)^2/4 - [P_0][S_0]}) \quad (1)$$

Here, P is the peptide, S is the substrate and PS the peptide substrate complex. The alternative solution to the second-order equation has been discarded because it can be shown to lead to concentrations of the PS complex that are close to $K_M$ even for very small concentrations of peptide and substrate. The initial rates of the hydrolysis of **I**, was measured for the peptide catalyst MNKR, and the results were fitted to eq 1 to obtain $k_{cat}$ and $K_M$. The hydrolysis of **I** catalyzed by MNKR showed saturation kinetics, with a $K_M$ of 0.001 M and a $k_{cat}$ of 0.000 17 $s^{-1}$, and

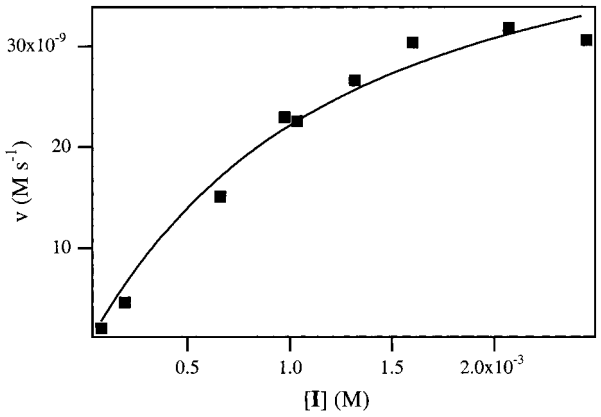


**Figure 6.** Plot of initial rate ($v$) of MNKR catalyzed hydrolysis of **I** at pH 5.1 and 290 K vs [**I**] at a peptide concentration of 0.3 mM and substrate concentrations of 0.05−2 mM. The solid line shows the best fit of the experimental data to eq 1, the Michaelis−Menten equation derived without the simplifying assumption that [S] ≫ [E].

thus a $k_{cat}/K_M$ of 0.17 $M^{-1}$ $s^{-1}$(Figure 6). This rate constant may be compared to the second-order rate constant for the 4-MeIm catalyzed hydrolysis of **I** which is 7.4 $10^{-4}$ $M^{-1}$ $s^{-1}$, and the ratio of $(k_{cat}/K_M)/k_2$ (4-MeIm) is 230 in aqueous solution at pH 5.1 and 290K. The peptide concentrations were 0.3 mM, and the substrate concentrations ranged from 0.05 mM to 2 mM. Although $K_M$ may formally reflect the build-up of an acyl intermediate, no observation of such an intermediate has been possible under reaction conditions despite several attempts by NMR and UV spectroscopy and by mass spectrometry.

Direct evidence for the formation of a peptide−substrate complex was achieved by $^1$H NMR spectroscopy. The $^1$H NMR spectrum of the amide and methyl regions of MNRK are shown in Figure 7 before and after addition of **I**. MNRK−substrate interactions are clearly visible in the amide and methyl regions under conditions where practically no chemical reaction has taken place, as shown by the virtual absence of free *p*-nitrophenol in the $^1$H NMR spectrum. The $^1$H NMR spectrum of the peptide MNII does not show the same changes, and the interaction is therefore peptide-specific and not, for example, due to the effect of the added acetonitrile. When the reaction proceeds, the methyl group resonances of MNRK are broadened further, probably due to complexation between the peptide and the reaction products. This can be compared to results from KO-42 catalyzed hydrolysis of **I** where the addition of 2 mM fumaric acid slows down the rate of peptide catalysis by 20% at pH 5.85.[18]

## Discussion

The four-helix bundle motif is the most widely studied in de novo design, both from a perspective of elucidating what sequences fold into well-defined tertiary structures,[1−3] and from the perspective of functionalization.[8−14] In the designed four-helix bundle catalyst KO-42, surface exposed histidines catalyze hydrolysis and transesterification reactions of *p*-nitrophenyl esters with second-order rate constants that are 3 orders of magnitude larger than those of the corresponding 4-MeIm catalyzed reactions.[18,19] The reactive entity consists of one unprotonated and one protonated His residue in positions *i, i-4* in a helical conformation, and the reactivity of the $HisH^+$−His pair can be calculated from the reactivity and p$K_a$ of 4-MeIm and from the p$K_a$ values of the histidines using the Brønsted equation with the coefficients $\beta = 0.8$ and $\alpha = 0.6$.[19] It increases with the nucleophilicity of the unprotonated residue, and the acidity of the protonated residue and the reactivity of the $HisH^+$−His site, relative to that of 4-MeIm, at a pH below the p$K_a$ of the histidines, therefore increases as the p$K_a$ of the His residues decrease. An increase in reactivity at a given pH must therefore come from transition-state binding by side chains of amino acid residues that flank the $HisH^+$−His site.

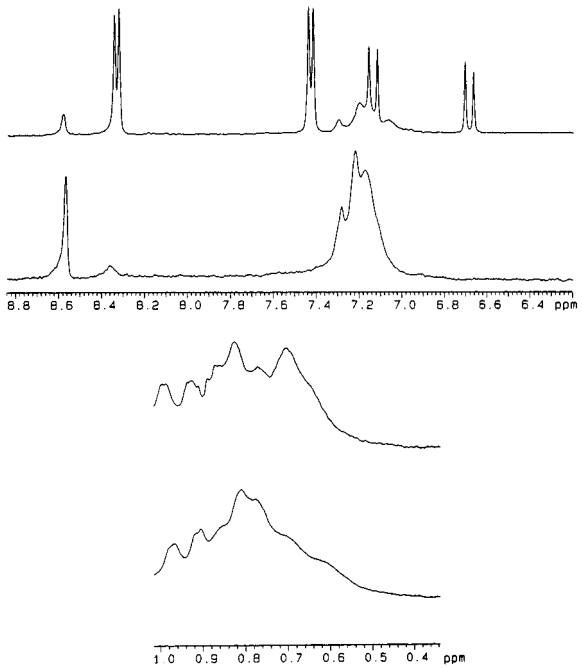


**Figure 7.** Part of the amide and methyl regions of the $^1$H NMR spectrum of MNRK at pH 5.1 and 293 K in 100 mM sodium acetate-$d_4$ buffer before (lower trace) and immediately after (upper traces) the addition of **I**. The concentration of peptide was approximately 0.4 mM and that of **I**, 1.5 mM. The spectral changes upon addition of **I** are clearly seen in the methyl region of MNRK, and the lack of free *p*-nitrophenol resonances shows that the reaction has not proceeded to any measurable degree.

The cooperative catalysis of acyl-transfer reactions by two His residues in a helix imposes stereochemical limitations on the structure of the transition state. The developing covalent bond between the nucleophile and the carbonyl carbon and the hydrogen bond between the general acid and one or both of the ester oxygens are expected to be roughly aligned with the helical axis. In a four-helix bundle motif, the side chains of residues in the adjoining helix are therefore suitable targets for the introduction of functionality that can bind the acyl or the leaving groups, and increased reactivity provides an assay by which such interactions can be identified. The distance between the centers of two helices in a well-packed helix-loop-helix motif is approximately 10 Å, and in a disordered one, it is longer. To achieve interactions between residues in separate helices, only the residues that are oriented toward the adjoining helix can be used. In fact, the observation of such interactions would provide a measure of the distance between these residues.

The MN-42 catalyzed hydrolysis of **II** in aqueous solution at pH 5.1 proceeds with a second-order rate constant of 0.030 $M^{-1}$ $s^{-1}$, Figure 2. MN-42 has three His residues in helix I, but no residues in helix II that are capable of binding. Introduction of Arg or Lys or combinations of the two in positions 30 and 34 invariably increase the rate constant, most strikingly in MNRK where Arg-30 and Lys-34 have been introduced and where the second-order rate constant is 0.106 $M^{-1}$ $s^{-1}$ and thus larger than that of MN-42 by a factor of 3.5. The introduction of the two binding residues thus reduces the

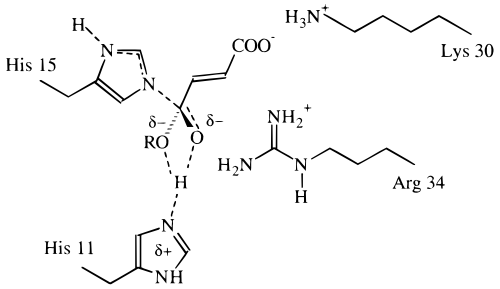


**Figure 8.** Proposed structure of the transition state of MNKR catalyzed hydrolysis of **I** based on the experimental results.

free energy of activation by 0.75 kcal/mol. Since **II** has no ionizable groups, we conclude that the positively charged binding residues bind the developing oxyanion as the substrate approaches the tetrahedral intermediate.

The second-order rate constants for the peptide catalyzed hydrolysis of **I** are invariably larger than or equal to those of **II**, and the rate constant ratios approach a factor of 2 in the cases of MNKR and MNRR, two of the more efficient catalysts, Figure 2. In the MNKR catalyzed reaction, the extra transition-state stabilization amounts to 0.4 kcal/mol, a value that is close to what is observed for surface-exposed salt bridges in folded polypeptides and therefore what can be expected from a well positioned binding residue. The observation of the reduction in the free energy of activation by almost the full amount of a salt bridge suggests that the geometry of the transition state fits better in the reactive site than that of the substrate. However, the fact that saturation kinetics are obtained and therefore that the substrate is bound by MNKR suggests that the total binding energy of the transition state is larger. The binding of the carboxylate residue of **I** by MNKR appears to be highly specific because, when Lys-30 is replaced by Orn-30, the discrimination between **I** and **II** disappears. A proposed transition-state structure based on the results is shown in Figure 8. The discrimination may also prove to be larger for longer amino acid side chains in the binding residues of helix II.

The direct assignment of binding interactions to individual amino acid residues is complicated by what seems to be interactions between the binding amino acids. Lys-30 in combination with Gln-34 in MNKQ does not enhance the rate of hydrolysis beyond that of MN-42 which has no binding residues in helix II, yet the introduction of Lys-30 next to Arg-34 in MNKR increases the reactivity in comparison to that of Arg-34 in MNQR by a factor of 2. Also, the replacement of Arg-30 or Arg-34 in MNRR by Lys-30 or Lys-34 increases the second-order rate constants in MNKR and MNRK. The interplay between the binding residues in helix II is not clear but may be due to charge−charge repulsions that force the binding residues to adopt nonoptimal binding geometries.

In our system, the binding site for ester hydrolysis is structurally well-defined; only a limited number of positions in the adjoining helix can be used to enhance the reactivity of the peptide catalysts. In the JNII series of peptides, where there is only a single well-defined $HisH^+$−His site, Arg-11 and Arg-15 enhance the reactivity by almost a factor of 2. Arg-8−Lys-11 and Arg-11−Lys-8 have negligible effects on the second-order rate constants, those of JNII, $JNIIK_8R_{11}$, and $JNIIR_8K_{11}$ are virtually the same.

Hydrophobic interactions can be expected to provide considerably larger binding energies than electrostatic ones, the binding energy of the side chains of, for example, Leu in enzymes catalyzing the biosynthesis of proteins amount to several kcal/mol.[28] The exploitation of hydrophobic recognition by the four-helix bundle motif is therefore a key ingredient in the development of efficient designed catalysts. The observed rate enhancement in the JNIII catalyzed hydrolysis of fatty acid esters upon lengthening the aliphatic chain by three carbon atoms is larger than one order of magnitude and corresponds to 1.6 kcal/mol of excess binding energy in the transition state. The rate enhancement is an approximately linear function of chain length which shows that the free energy gain per methylene group tends toward a maximum value. This is not unexpected since the differentiation between transition-state binding and ground-state binding should decrease with the distance from the reactive site. Nevertheless, hydrophobic binding appears to be a functional design idea in the engineering of surface catalysts.

The observed rate enhancements $k_2$ (**III**)/$k_2$ (**I**) are less for JNI and JNII than for the JNIII catalyzed reactions, and the geometric constraints from the $HisH^+$−His pair are apparently quite strong. With only His-34 as the nucleophile and no binding interactions from His-30, the hydrophobic effect can be more efficiently utilized probably because the geometry of the transition state can adjust to allow a better fit of the hydrophobic residues in the binding site. The observation of more efficient hydrophobic binding in the His-34 catalyzed reaction is compatible with the fact that His-34 is close to the hydrophobic residues as shown by the identification of NOE connectivities between His-34 and Ile-9, Leu-12, and Leu-31 in the $^1H$ NMR NOESY spectrum, Figure 5.

The geometry of the $HisH^+$−His site and the observation of recognition of carboxylate groups and of hydrophobic substituents, Figure 8, suggest the possibility of chiral discrimination between residues that have these structural components. Unfortunately, ester substrates that contain carboxylate anions tend to be very unstable due to efficient intramolecular catalysis, and monoesters of succinic or aspartic acids have short lifetimes in aqueous solution. We turned instead to the corresponding Lys substrate and its catalysis by MNEE. Unfortunately, the reactivity of MNEE is very low, and we could therefore not measure the peptide catalyzed reactions because they were masked by background hydrolysis. The observed chiral discrimination between D- and L-Nle is probably almost exclusively dictated by the inherent constraints from the $HisH^+$−His pair and due to charge repulsion between positively charged residues. The cationic amino group of the L-Nle ester probably experiences stronger repulsive interactions from the positively charged Arg and Lys in positions 30 and 34 than that of the D-ester. Nevertheless, the observation of chiral discrimination by rational design is clearly gratifying. The number of possible reaction pathways must, however, be further reduced in order to achieve larger enantiomeric differences. Alternatively, the trapping of the acyl intermediate by chiral nucleophiles such as amino alcohols or peptides may generate larger enantiomeric excesses.

The magnitudes of the rate enhancements caused by the introduction of Arg and Lys and by the recognition of hydrophobic residues are satisfying, considering that they are due to a small number of interactions between the substrate and one or two residues. The active sites of efficient biocatalysts contain a multitude of residues organized in three-dimensional space capable of hydrogen bonding and other electrostatic interactions with the substrate. The incorporation of further binding residues in designed polypeptide catalysts can therefore be expected to enhance rates even further. However, more

(28) Fersht, A. *Enzyme Structure and Mechanism*; 2nd ed.; W. H. Freeman and Company: New York, 1985.

importantly, the precise incorporation of residues that bind cooperatively provides binding energies in excess of the sums of the participating species. Synergic effects among many residues that bind with modest energies may therefore prove to be more important than the introduction of individual strongly binding interactions, although the latter may be more tempting. Consequently, the binding energies obtained here pave the way for the further development of designed catalysts. Whether that development takes place on the surface of a folded polypeptide or of another biomolecule or in a cavity of a protein remains a prospect for the future. The NMR spectroscopic results show that the surface-exposed residues of the peptide catalysts are not held in fixed positions, a factor that may limit the catalytic efficiency of surface catalysts.

Interestingly, the introduction of binding residues that enhanced the reactivity led to a catalyst that exhibits saturation kinetics. As a natural consequence of increasing the transition-state binding, stronger ground-state binding followed, Figure 6. A $K_M$ of 1 mM is comparable to those of many natural biocatalysts and also to those of other designed catalysts. It can therefore be concluded that the binding strength is sufficient for efficient catalysis, and that $k_{cat}$ should be the main target for redesign. The strong binding of **I**, on the surface of a four-helix bundle is perhaps surprising, and corroborative evidence was therefore acquired. The observation by NMR spectroscopy that **I** binds to MNRK at submillimolar concentrations of peptide and substrate with clearly observable chemical shift effects on residues in the hydrophobic core implies that hydrophobic interactions coupled to charge−charge interactions may be involved. The structure of the peptide−substrate complex cannot be obtained due to fast exchange, but hydrophobic binding is strongly suggested by the chemical shifts of the residues in the hydrophobic core of the folded motif. The corresponding effects on the surface-exposed residues are not equally informative since they are small due to shift-averaging on the surface of the helix-loop-helix motif.

With the observations of the formation of a peptide−substrate complex, a rate-limiting formation of an acyl intermediate that can be trapped by nucleophiles, and the dependence of reaction rate on pH, a free energy diagram of MNKR catalyzed hydrolysis of **I** could be constructed. The evidence for the formation of a peptide−substrate complex comes from the direct measurement of saturation kinetics and from direct observation by NMR spectroscopy. The structure of the transition state with an unprotonated His nucleophile flanked by a protonated His residue is concluded from the pH dependence and from the observation of kinetic isotope effects.[19] The binding of the developing oxyanion and of the fumaryl carboxylate anion has been established by the structure−function relationships reported here. The observation that the nature of the reaction products depends on the presence of nucleophiles shows that there is an intermediate on the reaction pathway and that this most likely is an acyl imidazole. Since it does not accumulate, it does not impede the overall reaction. Finally, the release and the identity of the reaction products have been demonstrated by NMR spectroscopy. The rationally designed four-helix bundle catalyst MNKR is therefore characterized by the complexity of native enzymes, and the relationship between structure and function is well understood. $K_M$ is quite satisfactory for efficient catalysis but $k_{cat}$ remains to be optimized further.

**Conclusion.** We have shown by rational design that four-helix bundle catalysts can be engineered to have the capability of catalyzing the hydrolysis of *p*-nitrophenyl esters with rate enhancements approaching three orders of magnitude, substrate recognition, chiral discrimination, and saturation kinetics. Thus these catalysts are capable of all the complexities of the naturally occurring biocatalysts, although the rate enhancements are far from those that occur in nature. Binding energies are surprisingly large, considering that the sites are located on the surface of folded four-helix bundle proteins and exposed to solvent water with a high dielectric constant and in competition with hydrogen bonding from the solvent molecules. The observed substrate recognition is the first reported example in a designed polypeptide with an adopted tertiary fold where individual substrates are specifically recognized by the catalyst.

## Experimental Section

**Peptide Synthesis.** The peptides were synthesized on a Perseptive Pioneer automated peptide synthesizer using a standard PerSeptive Biosystems Fmoc protocol and an Fmoc-PAL-PEG-PS polymer (PerSeptive Biosystems) that leaves the cleaved peptide amidated at the C terminus. The peptide N-terminals were capped by acetic anhydride. Peptides were cleaved from the polymer and deprotected in a mixture of TFA (9 $\mu$L), anisole (200 $\mu$L), ethanedithiol (300 $\mu$L), and thioanisole (500 $\mu$L) per gram of polymer, for 2 h at room temperature, precipitated by cold diethyl ether, and lyophilised. They were purified by reversed-phase HPLC on a semipreparative C-8 Kromasil column, eluted isocratically with 39 to 43% 2-propanol in 0.1% TFA at a flow rate of 5 mL/min. The purity was checked by analytical HPLC under similar conditions, and the peptides were identified by electrospray mass spectrometry (ES-MS). Typical measured molecular weights were within 1 mu from the calculated ones, and after HPLC purification, no high molecular weight impurities were detected in the ES-MS spectrum.

**NMR and CD Spectroscopy.** 1D $^1$H NMR spectra were recorded at 400 MHz using a Varian Unity 400 NMR spectrometer at peptide concentrations of approximately 0.4 mM. The identification of a peptide−substrate complex formed from MNRK and **I** was performed in 90% $H_2O$/10% $D_2O$ at pH 5.1 (uncor) and 293 K. The peptide solution (0.4 mM, 650 $\mu$L) was temperature-equilibrated, and spectra were recorded immediately before and after the addition of 50 $\mu$L of a saturated solution of **I** in 50% acetonitrile-$d_6$/50% 100 mM sodium acetate-$d_3$ buffer. NOESY and TOCSY spectra were recorded at 500 MHz on a Varian Inova 500 NMR spectrometer operating at 313 K, and peptide solutions were approximately 1 mM in 90%$H_2O$/10%$D_2O$ at pH 5. The 90° pulses were 4.6 ms, spin-lock pulses were 20 ms, sweep widths were 6500 Hz, and 2 *256 increments were recorded and processed using linear prediction in the indirect dimension.

CD spectra were recorded on a Jasco J-720 spectrometer, routinely calibrated with (+)-camphor-10-sulfonic acid. The samples were prepared in buffer solution, and peptide concentrations were determined by quantitative amino acid analysis. Typical CD spectra were measured using 0.1-mm cuvettes at pH 5.1 in 100 mM sodium acetate in the wavelength interval 260 to 200 nm.

**Kinetic Measurements.** The kinetic measurements were carried out by using Varian Cary 1 or Cary 4 spectrophotometers equipped with Varian temperature controllers and by following the absorbance of released *p*-nitrophenol at 320 nm. The samples were prepared from a pH-adjusted and centrifuged stock peptide buffer solution and diluted to the desired concentrations, and the concentrations of the peptide stock solutions were determined by quantitative amino acid analysis. In a typical kinetic experiment, 270 $\mu$L of the peptide solution (0.2−0.4 mM) was temperature-equilibrated in a 1-mm cuvette, after which 5 $\mu$L of the substrate solution (7.4 mM) was added to give a substrate concentration of 0.13 mM.

The substrates **I**, L-**IV** and D-**IV** were dissolved in 50% acetonitrile/50% buffer, and the fatty acid esters were dissolved in 100% acetonitrile. Peptide catalyzed hydrolyses of **I** and **II** were performed in parallel with samples prepared from the same peptide stock solutions to avoid interexperimental errors from quantitative amino acid analysis. The rate constants reported are the results from linear regression analysis of the experimentally measured pseudo-first-order rate constants as a function of three or more peptide concentrations.

The relative rates for MN-42 and JN-42 catalyzed hydrolysis of fatty acid esters were measured with samples prepared from a common

peptide stock solution. The relative rates for peptide catalyzed hydrolysis of D-**IV** and L-**IV** were measured by splitting a peptide stock solution into two cuvettes, adding D-**IV** to one cuvette and L-**IV** to the other, and measuring the release of *p*-nitrophenol at 320 nm. After the reaction was complete, a second addition of substrate was made with D-**IV** added to the cuvette where L-**IV** was initially added, and vice versa, to minimize interexperimental errors, and the reaction rate was again measured. The reported second-order rate constants are the mean value of two experiments after correction for background hydrolysis. The rate constants for the background hydrolysis of D-**IV** and L-**IV** were measured several times, and the individual rate constants did not differ by more than 5%. All second-order rate constants reported for 4-methyl imidazole catalyzed reactions are the results from linear regression using three or more different concentrations of catalyst.

In the initial rate experiments, a peptide stock solution was prepared with a concentration of approximately 0.3 mM at pH 5.1 in 100 mM sodium acetate buffer. Six cuvettes with varying volumes of peptide stock solution were temperature-equilibrated at 290 K in the sample compartment of the UV spectrophotometer. The remainder of the peptide stock solution was also temperature-equilibrated as was an Eppendorf tube with a weighed quantity of **I**. Immediately prior to starting the experiment, the peptide stock solution was added to the substrate, the tube was briefly vortexed, and undissolved **I** was spun down. The appropriate volumes of the peptide solution, saturated with **I**, were added quickly to the cuvettes, and the release of *p*-nitrophenol was measured at 320 nm after a brief shaking of each cuvette. The substrate **I** was soluble to about 2 mM under those conditions.

The concentrations of substrate varied from about 0.05 mM to saturated (2 mM). Quantitative amino acid analysis after the kinetic runs was used to verify that no peptide precipitation occurred with the excess substrate. The reactions were typically followed for 30 min, and data points recorded during the first 20 min were used in the calculation of the initial rate. The amount of substrate in each cuvette was determined by withdrawing 150 $\mu$L by pipet and transferring it into a 5-mL measuring flask. The substrate was then completely hydrolyzed by the addition of 0.1 M NaOH. The absorbance at 405 nm due to the *p*-nitrophenoxide ion was measured in a 1-cm cuvette, and the concentration was calculated using a previously determined extinction coefficient $\epsilon = 17\,840\ M^{-1}\ cm^{-1}$. The initial rate ($v$) was fitted to eq 1, and the values of $K_M$ and $k_{cat}$ were obtained from the best fit of the experimental data.

**Synthesis of Substrates.** The synthesis of mono-*p*-nitrophenyl fumarate has been described previously.[29] The *p*-nitrophenyl esters of D- and L-Nle were synthesized from D- and L-Nle, respectively, using standard procedures. The α-amino groups were protected by the benzyloxycarbonyl group using 1.1 equiv of benzyl chloroformate in alkaline aqueous solution at 10 °C. The carboxylic acid was esterified with 1.1 equiv of *p*-nitrophenol, 1.1 equiv of dicyclohexylcarbodiimide and 0.1 equiv of 4-pyrrolidinopyridine. Finally, the α-amino group was deprotected using 33% HBr in acetic acid, and the resulting salt was precipitated with diethyl ether. The purity of each product was checked with $^1$H NMR spectroscopy, where the aromatic proton resonances of the *p*-nitrophenyl esters are diagnostic of ester formation and the spin systems of the amino acids are readily assigned. The *p*-nitrophenyl esters of the enantiomers of lysine were synthesized and identified in a similar manner.

**Acknowledgment.** We are indebted to Dr. Gunnar Stenhagen for expert mass spectrometric assistance, to Dr. Linda Cammish, Per Septive Biosystems, for the synthesis of several of the MN series of peptides. Financial support from the Swedish Natural Science Research Council and from Carl Tryggers Foundation is gratefully acknowledged. We thank the Swedish NMR Centre at Göteborg University for the use of a 500-MHz NMR spectrometer.

JA980682E

(29) Baltzer, L.; Lundh, A.-C.; Broo, K.; Olofsson, S.; Ahlberg, P. *J. Chem. Soc., Perkin Trans. 2.* **1996**, 1671−1676.